Experimental Modal Analysis

Gaetan Kerschen - Jean-Claude Golinval

1 An Introduction to Experimental Modal Analysis

Vibrations are ubiquitous in everyday life. They may often have undesirable effects such as noise disturbances or may even cause the ruin of a structure. The last three decades have thus witnessed a tremendous interest in a better understanding of the structural dynamic behaviour, and identifying the modal parameters, namely the natural frequencies, damping ratios and mode shapes, has become a major concern of structural dynamicists. This field of research is referred to as *modal analysis* in the technical literature [1, 2, 3] and relies on two important assumptions: linearity and time invariance of the structure. The knowledge of the modal parameters can serve various purposes including structural modification [3], assessment of the structural integrity and reliability [4], structural health monitoring [5] and model updating [6].

Two different ways exist for calculating the modal parameters (see Figure 1). The first method called theoretical modal analysis assumes the knowledge of the structural matrices, namely the stiffness matrix $\mathbf{K}$, the mass matrix $\mathbf{M}$ and the damping matrix $\mathbf{C}$. It merely consists in solving an eigenvalue problem. For instance, in the undamped case, the natural frequencies ω_i and mode shapes $\mathbf{x}_{(i)}$ are such that:

$$(\mathbf{K} - \omega_i^2 \mathbf{M})\mathbf{x}_{(i)} = 0 \tag{1}$$

if ω_i^2 is a root of the algebraic equation:

$$\det(\mathbf{K} - \omega^2 \mathbf{M}) = 0 \tag{2}$$

The second approach called experimental modal analysis exploits the system response and involves modal analysis identification techniques for the computation of the modal parameters. Since a mathematical model of an existing structure is not always available, this second alternative has received increasing attention in recent years. Accordingly, a lot of research has been conducted with the aim of developing robust methods.

Modal analysis identification techniques can be broadly classified according to three criteria:

1. The system response can be measured either in the time domain (e.g., accelerations) or in the frequency domain (e.g., frequency response functions (FRFs)). The key advantage of frequency domain identification techniques is that the accuracy of the results can be improved by adding residual terms. However, problems such as leakage or closeness of natural frequencies should be treated carefully. This the reason why time domain methods have also enjoyed a certain popularity.

2. A distinction can be made between single-degree-of-freedom (SDOF) and multi-degree-of-freedom (MDOF) methods depending on the number of modes which can be taken into account in the analysis. In the time domain, it is generally not possible to separate the contributions from the different modes and an MDOF analysis has to be performed.

3. Some frequency domain methods (single-input-single-output (SISO) methods) cannot deal with FRFs from several response locations at the same time whereas other methods can (single-input-multi-output (SIMO) methods). The structure can also

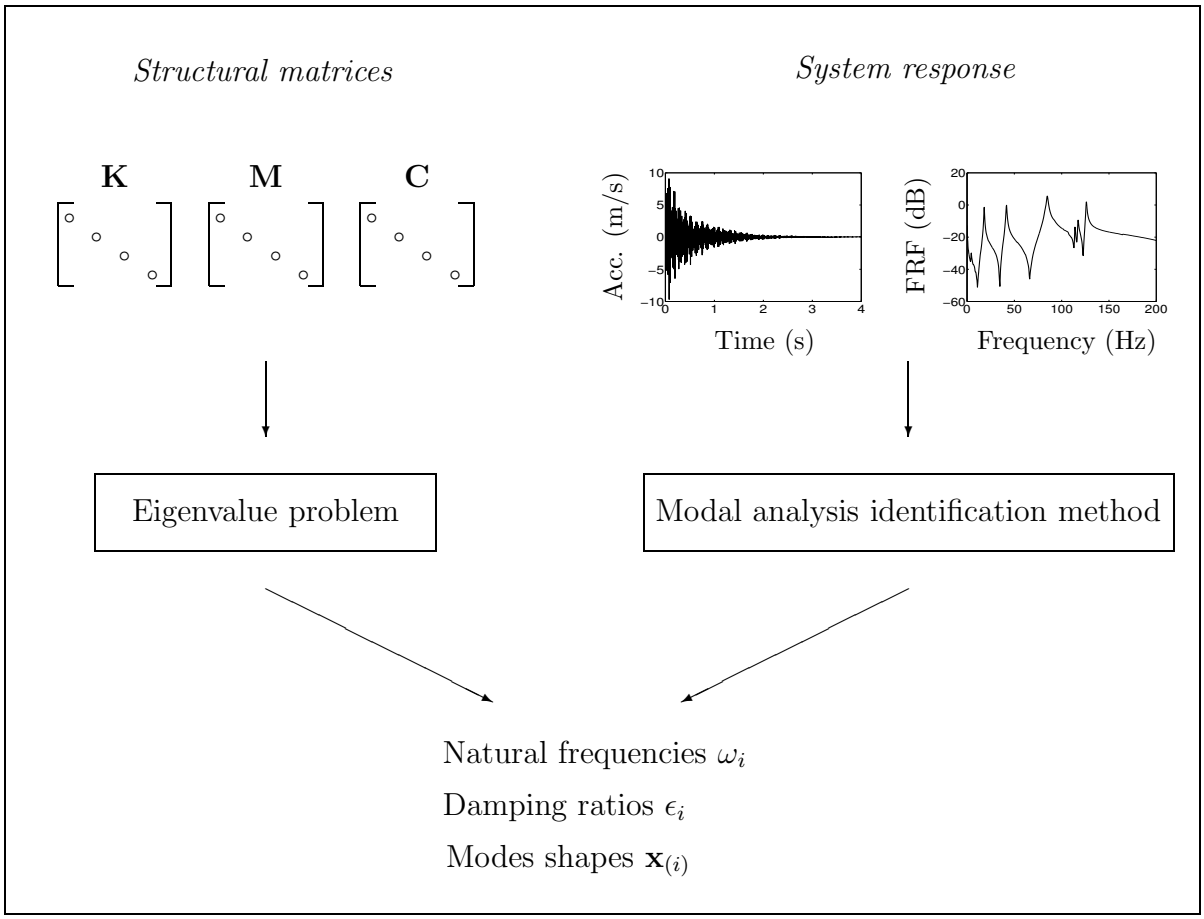

Figure 1: Theoretical and experimental modal analysis.

be excited at several points simultaneously but this is the exception rather than the rule.

Numerous identification methodologies have been proposed in the literature. In the present chapter, the analysis is however restricted to those which are the most widely used:

1. The first method investigated is the Least-Squares Complex Exponential method which was introduced in 1979 by Brown *et al.* [7]. It requires the measurements of impulse response functions (IRFs) and yields the natural frequencies and damping ratios. It is often coupled with the Least-Squares Frequency Domain technique in order to obtain an estimation of the mode shapes.

2. The second method is the Ibrahim Time Domain method which was proposed in 1973 by Ibrahim and Mikulcik [8]. It exploits free response time histories from the structure under test.

3. The third method is the Stochastic Subspace Identification method which has been recently introduced [9]. It is known to outperform the classical identification techniques.

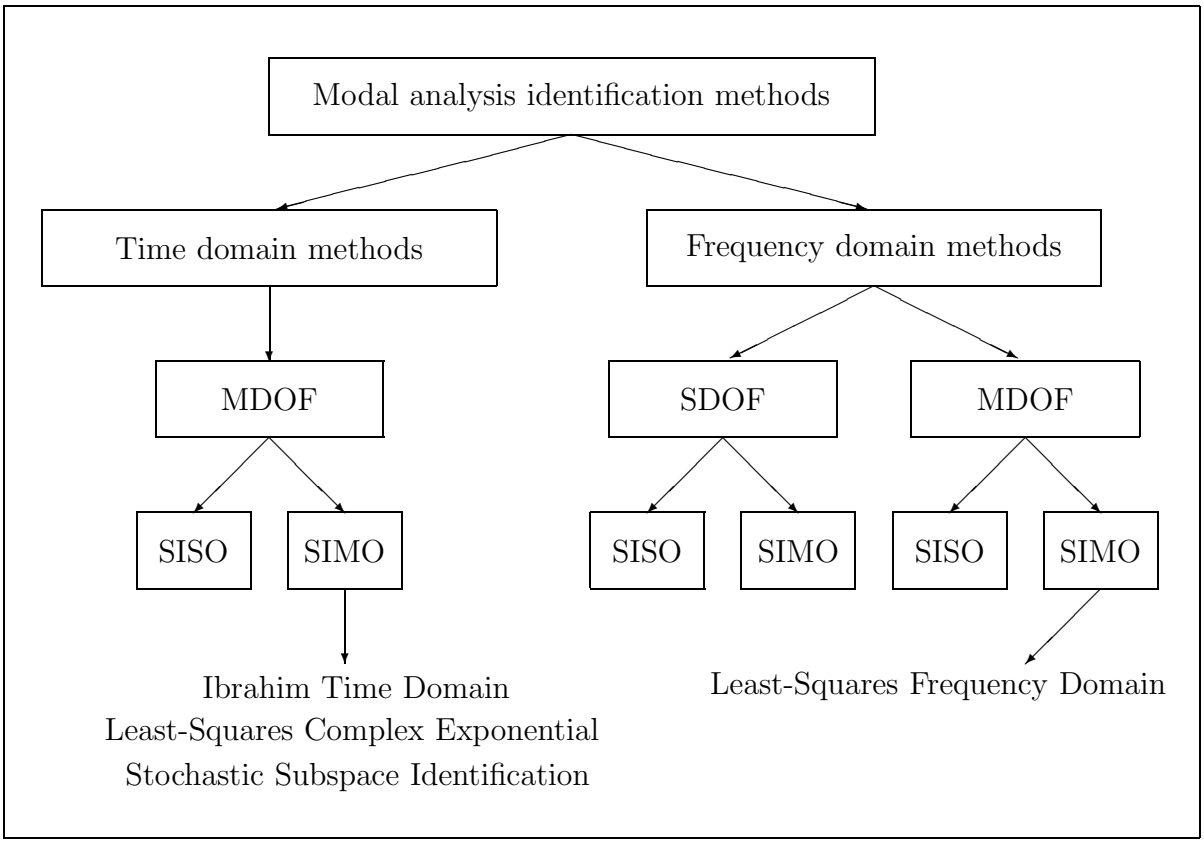

Figure 2: Classification of identification methods.

The characteristics of these methods are summarised in Figure 2.

In order to gain some insights into the practical application of the methods, they are applied to a benchmark structure built to simulate the dynamic behaviour of an aeroplane. The structure has been proposed as a benchmark study in the framework of the European COST Action F3 [10] but has also been built at the University of Liège (Figure 3). The structure is composed of steel beams with rectangular cross-sections, and lumped masses are used to represent the engines. A low frequency suspension ensures the free-free boundary conditions. In order to increase the damping, a viscoelastic tape was bonded to the wings and covered by a thin aluminium constraining layer.

The measurements have been carried out using eleven accelerometers. Eight accelerometers span the wings regularly, two are located on the horizontal stabiliser and one on the vertical stabiliser. The structure has been excited using a hammer impact at the wing tip. Two different test data sets have been made available. The first set consists of time histories (2048 points) sampled at 512 Hz. The second set consists of FRFs with 801 points up to 200 Hz. By way of illustration, the data at sensor 1 (wing tip) is represented in Figure 4.

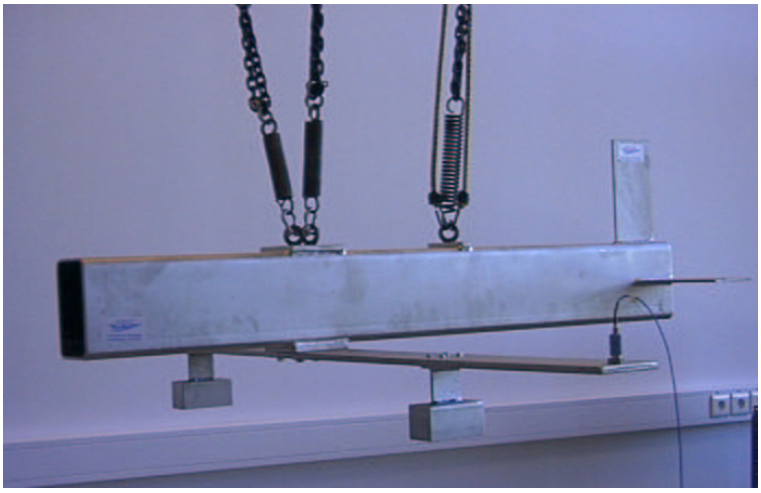

Figure 3: Aeroplane-like structure.

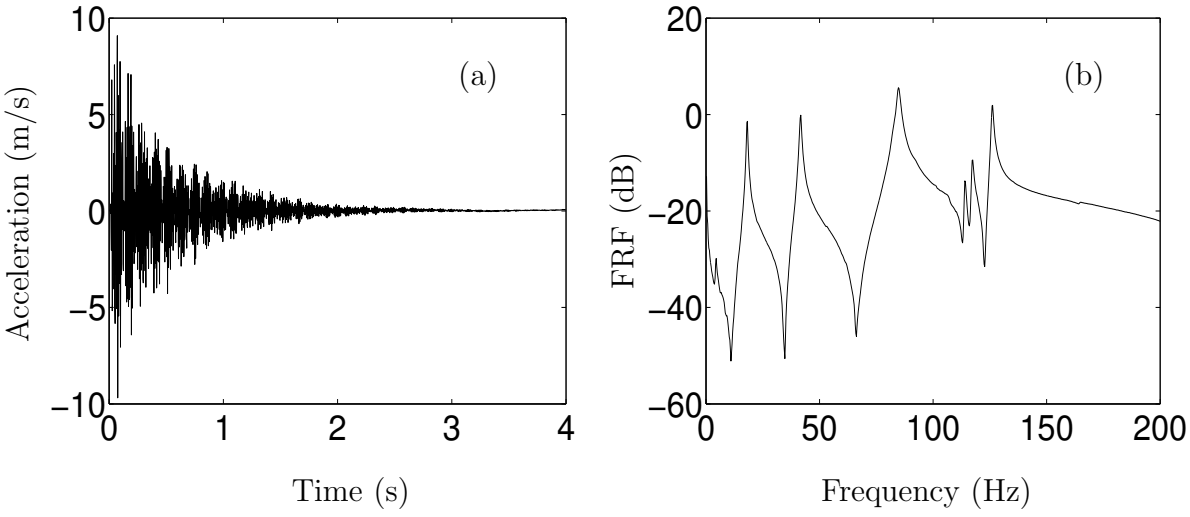

Figure 4: Measured data at sensor 1. (a) Acceleration signal; (b) FRF.

2 Least-Squares Complex Exponential and Frequency Domain Methods

2.1 Least-Squares Complex Exponential Method

A popular form of curve-fitting experimental data is the Least-Squares Complex Exponential method (LSCE). It calculates the system poles λ_k in the time domain by making use of impulse response functions (IRFs) obtained from FRFs by an inverse Fourier transform (IFFT):

$$\begin{aligned} h_{rs}(t) &= \text{IFFT}\left[H_{rs}(\omega)\right] \\ &= \text{IFFT}\left[\sum_{k=1}^{n}\left(\frac{A_{rs(k)}}{i\omega-\lambda_k}+\frac{\bar{A}_{rs(k)}}{i\omega-\bar{\lambda}_k}\right)\right] \\ &= \sum_{k=1}^{n}\left(A_{rs(k)}e^{\lambda_k t}+\bar{A}_{rs(k)}e^{\bar{\lambda}_k t}\right) \\ &= 2Re\left[\sum_{k=1}^{n}A_{rs(k)}e^{\lambda_k t}\right] \end{aligned} \tag{3}$$

with the residue $A_{rs(k)}=\frac{z_{r(k)}z_{s(k)}}{\rho_k}$ defining the displacement of the rth degree-of-freedom in the sth mode. A bar denotes the complex conjugate.

The FRFs are generally measured with a constant sampling frequency FS thereby giving IRFs sampled at equally-spaced time intervals $\Delta t = 1/FS$:

$$h_{rs}(j\Delta t)=2Re\left[\sum_{k=1}^{n}A_{rs(k)}e^{\lambda_k(j\Delta t)}\right]=2Re\left[\sum_{k=1}^{n}A_{rs(k)}V_k^j\right] \tag{4}$$

where the abbreviation $V_k=e^{\lambda_k\Delta t}$ is used for convenience.

In order to explain how the system poles λ_k are computed from the measured IRFs, autoregressive moving average (ARMA) models need to be introduced. Let us consider a SISO model in the frequency domain:

$$H_{rs}(\omega)=\frac{Q_r(\omega)}{P_s(\omega)}=\frac{\alpha_{o_p}(i\omega)^{o_p}+\alpha_{o_p-1}(i\omega)^{o_p-1}+...+\alpha_1(i\omega)^1+\alpha_0(i\omega)^0}{\beta_{o_q}(i\omega)^{o_q}+\beta_{o_q-1}(i\omega)^{o_q-1}+...+\beta_1(i\omega)^1+\beta_0(i\omega)^0}=\frac{\sum_{j=0}^{o_p}\alpha_j(i\omega)^j}{\sum_{j=0}^{o_q}\beta_j(i\omega)^j} \tag{5}$$

Further rearranging yields the following equation:

$$\sum_{j=0}^{o_q}\beta_j(i\omega)^j Q_r(\omega)=\sum_{j=0}^{o_p}\alpha_j(i\omega)^j P_s(\omega) \tag{6}$$

The time domain model which corresponds to the SISO frequency domain model is known as an ARMA model:

$$\sum_{j=0}^{o_q}\beta_j\ q_r(t+j\Delta t)=\sum_{j=0}^{o_p}\alpha_j\ p_s(t+j\Delta t) \tag{7}$$

If the discussion is limited to the use of free decay or IRF data, the previous time domain equation can be simplified by noting that the forcing function $p_s(t)$ can be assumed to be zero for all time greater or equal to zero:

$$\sum_{j=0}^{o_q} \beta_j \; h_{rs}(t + j\Delta t) = 0 \tag{8}$$

If t is taken as equal to 0, equation (8) becomes:

$$\sum_{j=0}^{o_q} \beta_j \; h_{rs}(j\Delta t) = 0 \tag{9}$$

and by plugging equation (4) into equation (9):

$$\sum_{j=0}^{o_q} \beta_j \; 2Re\left[\sum_{k=1}^{n} A_{rs(k)} V_k^j\right] = 2Re\left[\sum_{k=1}^{n} A_{rs(k)} \sum_{j=0}^{o_q} \beta_j V_k^j\right] = 0 \tag{10}$$

This equation shows that there always exists a polynomial in V_k of order o_q with real coefficients β_j such that the following relation is verified:

$$\beta_0 + \beta_1 V_k + ... + \beta_j V_k^j + ... + \beta_{o_q} V_k^{o_q} = 0 \tag{11}$$

Equations (9) and (11) allows us to compute the natural frequencies and damping ratios using a two-step procedure:

1. Determine the coefficients β_j by using equation (9) and assuming that $\beta_{o_q} = 1$:

$$\begin{bmatrix} h_{rs}(0) & h_{rs}(\Delta t) & ... & h_{rs}((o_q-1)\Delta t) \\ h_{rs}(\Delta t) & h_{rs}(2\Delta t) & ... & h_{rs}(o_q\Delta t) \\ \vdots & \vdots & ... & \vdots \\ h_{rs}((o_q-1)\Delta t) & h_{rs}(o_q\Delta t) & ... & h_{rs}((2o_q-2)\Delta t) \end{bmatrix} \begin{bmatrix} \beta_0 \\ \beta_1 \\ \vdots \\ \beta_{o_q-1} \end{bmatrix} = - \begin{bmatrix} h_{rs}(o_q\Delta t) \\ h_{rs}((o_q+1)\Delta t) \\ \vdots \\ h_{rs}((2o_q-1)\Delta t) \end{bmatrix} \tag{12}$$

   It should be noted that noise disturbances can be averaged out by considering a number of measured values n_t much greater than the model order o_q. In that case, we end up with an overdetermined system to solve:

$$\begin{bmatrix} h_{rs}(0) & h_{rs}(\Delta t) & ... & h_{rs}((o_q-1)\Delta t) \\ \vdots & \vdots & ... & \vdots \\ h_{rs}((n_t-1)\Delta t) & h_{rs}(n_t\Delta t) & ... & h_{rs}((n_t+o_q-2)\Delta t) \end{bmatrix} \begin{bmatrix} \beta_0 \\ \vdots \\ \beta_{o_q-1} \end{bmatrix} = - \begin{bmatrix} h_{rs}(o_q\Delta t) \\ \vdots \\ h_{rs}((n_t+o_q-1)\Delta t) \end{bmatrix} \tag{13}$$

2. Determine V_k by finding the polynomial roots of equation (11). The system poles $\lambda_k = \omega_{0k}(-\epsilon_k \pm i\sqrt{1-\epsilon_k^2})$ are then easily computed since $V_k = e^{\lambda_k \Delta t}$:

$$\lambda_k = \frac{1}{\Delta t}(\ln|V_k| \pm i \arg(V_k)) \tag{14}$$

The extension of the previous procedure to a SIMO method, i.e., processing several IRFs from different response locations simultaneously, is straightforward in the sense the coefficients β_j do not depend on the particular IRF considered. For n_o response locations, the following system is to be solved:

$$\left[\begin{array}{cccc}
h_{11}(0) & h_{11}(\Delta t) & ... & h_{11}((o_q-1)\Delta t) \\
\vdots & \vdots & ... & \vdots \\
h_{11}((n_t-1)\Delta t) & h_{11}(n_t\Delta t) & ... & h_{11}((n_t+o_q-2)\Delta t) \\
\hline
h_{21}(0) & h_{21}(\Delta t) & ... & h_{21}((o_q-1)\Delta t) \\
\vdots & \vdots & ... & \vdots \\
h_{21}((n_t-1)\Delta t) & h_{21}(n_t\Delta t) & ... & h_{21}((n_t+o_q-2)\Delta t) \\
\hline
\vdots & \vdots & ... & \vdots \\
\hline
h_{n_o1}(0) & h_{n_o1}(\Delta t) & ... & h_{n_o1}((o_q-1)\Delta t) \\
\vdots & \vdots & ... & \vdots \\
h_{n_o1}((n_t-1)\Delta t) & h_{n_o1}(n_t\Delta t) & ... & h_{n_o1}((n_t+o_q-2)\Delta t)
\end{array}\right]
\left[\begin{array}{c} \beta_0 \\ \vdots \\ \beta_{o_q-1} \end{array}\right] =$$

$$-\left[\begin{array}{c}
h_{11}(o_q\Delta t) \\
\vdots \\
h_{11}((n_t+o_q-1)\Delta t) \\
\hline
h_{21}(o_q\Delta t) \\
\vdots \\
h_{21}((n_t+o_q-1)\Delta t) \\
\hline
\vdots \\
\hline
h_{n_o1}(o_q\Delta t) \\
\vdots \\
h_{n_o1}((n_t+o_q-1)\Delta t)
\end{array}\right] \tag{15}$$

2.2 Stabilisation Diagram

A crucial issue, also encountered with other identification techniques, is the selection of the correct model order o_q which is related to the number of assumed degree-of-freedom. If the analyst assumes a model order higher than the one actually present in the data, computational modes will result from the forced fulfillment of the specified model order rather than from dynamic system properties. To overcome this limitation, the identification is carried out for increasing model orders. All the solutions are combined in one single diagram called the stabilisation diagram, with as horizontal axis the pole frequency and as vertical axis the model order. Physical modes can then be easily separated from spurious modes by looking for poles which appear at nearly identical frequencies for the different model orders considered.

2.3 Least-Squares Frequency Domain Method

Contrary to other identification techniques, the LSCE method does not yield the mode shapes. In order to estimate these latter, a second method called Least-Squares Frequency Domain (LSFD) method is considered and takes advantage of the knowledge of the natural frequencies and damping ratios. The least-squares problem will be formulated in the frequency domain instead of the time domain mainly for two reasons:

- Start and end frequencies ω_{min} and ω_{max} can be specified which allows us to divide the frequency range in several intervals in which the coherence function has values near unity;
- Residual effects of modes outside the frequency band can be explicitly taken into account.

The method starts from the expression of the FRF:

$$H_{rs}(\omega) = \sum_{k=1}^{n} \left(\frac{A_{rs(k)}}{i\omega - \lambda_k} + \frac{\bar{A}_{rs(k)}}{i\omega - \bar{\lambda}_k} \right) + u_{rs} - \frac{l_{rs}}{\omega^2} \tag{16}$$

where the residual terms u_{rs} and l_{rs}/ω^2 correspond to stiffness and mass-like behaviours respectively. Expanding the residue $A_{rs(k)}$ into real and imaginary parts, i.e., $A_{rs(k)} = U_{rs(k)} + i\, V_{rs(k)}$, yields:

$$H_{rs}(\omega) = \sum_{k=1}^{n} \left\{ U_{rs(k)} \left(\frac{1}{i\omega - \lambda_k} + \frac{1}{i\omega - \bar{\lambda}_k} \right) + V_{rs(k)} \left(\frac{1}{i\omega - \lambda_k} - \frac{1}{i\omega - \bar{\lambda}_k} \right) \right\} + u_{rs} - \frac{l_{rs}}{\omega^2} \tag{17}$$

At this stage, the system poles λ_k are known and the values of $H_{rs}(\omega)$ are assumed to be measured. Accordingly, there are $2n+2$ unknowns: $U_{rs(1)}, ..., U_{rs(n)}, V_{rs(1)}, ..., V_{rs(n)}, u_{rs}$ and l_{rs}. Generally speaking, only the frequencies in a selected frequency interval $[\omega_{min}, \omega_{max}]$ are considered and an overdetermined system is to be solved provided that:

$$\frac{\omega_{max} - \omega_{min}}{\Delta\omega} + 1 > 2n + 2 \tag{18}$$

where $\Delta\omega$ and n are the frequency resolution and the number of modes in the frequency interval respectively.

The mode shapes must still be extracted from the residue $A_{rs(k)} = \frac{z_{r(k)} z_{s(k)}}{\rho_k}$ where a good approximation for ρ_k is $2i\,\omega_{0k}\,\mu_k$ [11]. By noting that $z_{s(k)} = \sqrt{i\, A_{ss(k)}}$, the expression for the ith component of the kth mode is obtained:

$$z_{r(k)} = \frac{A_{rs(k)} \sqrt{i}}{\sqrt{A_{ss(k)}}} \tag{19}$$

2.4 Relationship between Complex and Associated Real Modes Shapes

Due to the lack of a priori knowledge about dissipative phenomena, damping is rarely introduced in a finite element analysis. As a result, the finite element model is generally

undamped and the corresponding mode shapes are real. On the other hand, because damping is always present in real-life structures, experimental modal analysis yields complex mode shapes. This situation is thus embarrassing when the numerical and experimental modes are to be correlated.

It would be of particular interest to have a procedure which could deduce from the complex modes of a structure the associated real modes, i.e., the modes of the undamped system. This would also facilitate the visual representation of the experimental modes. To this end, let us recall the following expression [11]:

$$\mathbf{z}_{(k)} = \mathbf{x}_{(k)} + \sum_{s \neq k=1}^{n} i\omega_{0k} \frac{\beta_{ks}}{\mu_s(\omega_{0k}^2 - \omega_{0s}^2)} \mathbf{x}_{(s)} \tag{20}$$

which shows that the real part of the identified complex modes corresponds to the modes of the undamped system. It should however be borne in mind that equation (20) is valid when the damping is low and when the natural frequencies are well separated.

2.5 Application to an experimental structure

The LSCE method is now applied to the analysis of the dynamic characteristics of the aeroplane-like structure (see Figure 3). For the sake of conciseness, the study is limited in the 0-100 Hz range. The data set consists of eleven time histories of acceleration signals ($n_o = 11$) and 500 measured values are considered ($n_t = 500$).

The stabilisation diagram represented in Figure 5 shows the evolution of the identified natural frequencies with the model order o_q. To facilitate the extraction of the physical poles, the FRF measured at the horizontal stabiliser is superimposed. The natural frequency and the damping ratio of the stable poles are listed in Table 1. It should be noted that the damping ratios of the first and sixth modes are not very stable when the model order is varied.

Natural frequencies (Hz)	Damping ratios (%)
4.51	$\simeq$15
18.11	0.42
41.62	0.57
83.11	0.97
84.75	0.81
91.97	$\simeq$1.5
101.53	0.52

Table 1: Natural frequencies and damping ratios (LSCE method).

Now that an estimation of the system poles is available, the mode shapes can be identified using the LSFD method and the measured FRFs. They are represented in Figure 6. Mode 1 has not a clear structure and is in fact due to the low frequency suspension. This is also the reason why its damping ratio was so high and not very stable when the model order was increased. Mode 2 is therefore the first elastic deformation mode of the aeroplane and mainly involves wings bending. Modes 3, 4 and 5 are similar in the sense that they

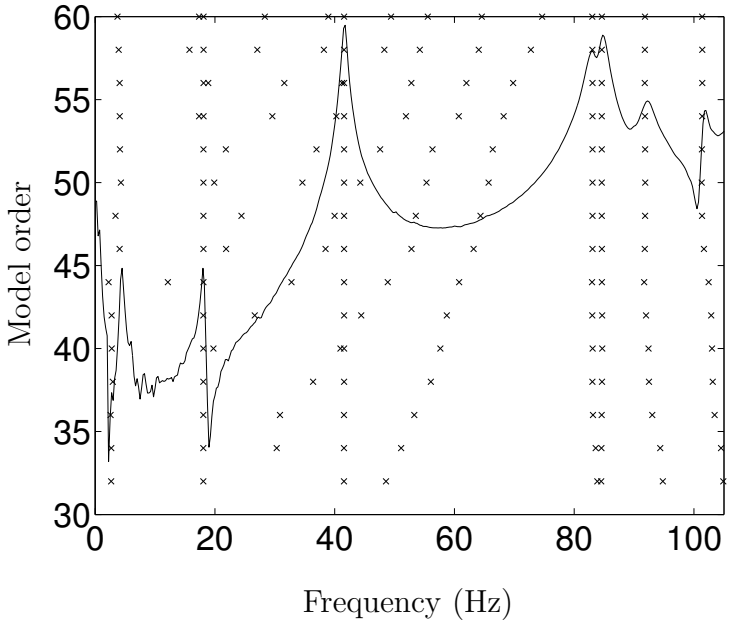

Figure 5: Stabilisation diagram.

all involve wings bending together with a rigid-body motion of the stabilisers. Finally, modes 6 and 7 are local modes of the stabilisers for which there is few deformation of the wings.

3 Ibrahim Time Domain Method

The Ibrahim Time Domain (ITD) technique considers free response time histories from the structure under test in order to determine its modal characteristics. The parameters are the natural frequencies, the damping factors and the mode shapes. This method has been introduced to avoid problems, e.g. modal interference of closely spaced modes, encountered using frequency domain methods. Among its numerous advantages, we can cite:

- It obtains the modal parameters in a single analysis;
- Either the acceleration, velocity or displacement response may be used;
- The use of the Fourier transform is not necessary and difficulties such as the leakage are avoided;
- A mathematical model of the structure is not developed;
- The input excitation does not need to be measured. However, care must be taken when acquiring the free responses. These latter have to be measured after the initial exciting force is removed.

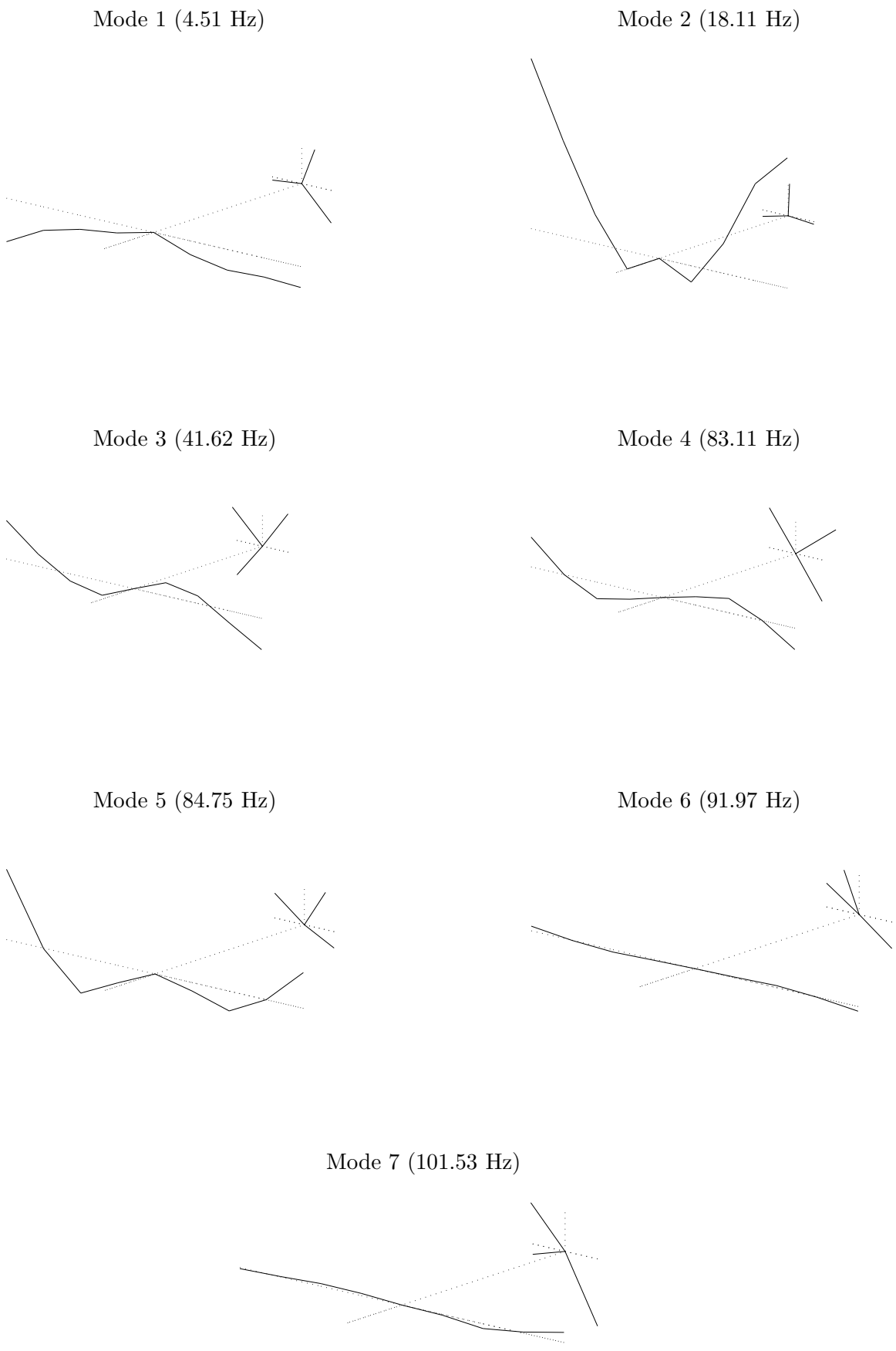

Figure 6: Representation of the mode shapes in the 0-100 Hz range (LSFD method).

3.1 Theoretical Background

The free response of a viscously damped linear system with n degree-of-freedom is governed by the following equations:

$$\mathbf{M}\ddot{\mathbf{q}}(t) + \mathbf{C}\dot{\mathbf{q}}(t) + \mathbf{K}\mathbf{q}(t) = 0 \tag{21}$$

where $\mathbf{M}, \mathbf{C}$ and $\mathbf{K}$ are the $n \times n$ structural matrices;
$\mathbf{q}$ is the vector of displacement co-ordinates.

The solution of this equation takes the form:

$$\mathbf{q}(t) = \sum_{k=1}^{2n} \mathbf{z}_{(k)}\, e^{\lambda_k t} \tag{22}$$

The system response may thus be viewed as an expansion in the modal basis $[\mathbf{z_{(1)}} \ ... \ \mathbf{z_{(2n)}}]$. If $2n$ time instants are considered, the data can be collected in a matrix $\mathbf{Q}$:

$$\underbrace{[\mathbf{q}(t_1) \ ... \ \mathbf{q}(t_{2n})]}_{\mathbf{Q}} = \underbrace{\left[\mathbf{z}_{(1)} \ ... \ \mathbf{z}_{(2n)}\right]}_{\mathbf{Z}} \underbrace{\begin{bmatrix} e^{\lambda_1 t_1} & \dots & e^{\lambda_1 t_{2n}} \\ \vdots & & \vdots \\ e^{\lambda_{2n} t_1} & \dots & e^{\lambda_{2n} t_{2n}} \end{bmatrix}}_{\mathbf{\Lambda}} \tag{23}$$

Let us consider now a second set of responses delayed by an interval Δt with respect to those of equation (23):

$$\begin{aligned} \underbrace{[\mathbf{q}(t_1 + \Delta t) \ ... \ \mathbf{q}(t_{2n} + \Delta t)]}_{\mathbf{Q}_{\Delta t}} &= \left[\mathbf{z}_{(1)} \ ... \ \mathbf{z}_{(2n)}\right] \begin{bmatrix} e^{\lambda_1 (t_1 + \Delta t)} & \dots & e^{\lambda_1 (t_{2n} + \Delta t)} \\ \vdots & & \vdots \\ e^{\lambda_{2n} (t_1 + \Delta t)} & \dots & e^{\lambda_{2n} (t_{2n} + \Delta t)} \end{bmatrix} \\ &= \left[\mathbf{z}_{(1)} e^{\lambda_1 \Delta t} \ ... \ \mathbf{z}_{(2n)} e^{\lambda_{2n} \Delta t}\right] \begin{bmatrix} e^{\lambda_1 t_1} & \dots & e^{\lambda_1 t_{2n}} \\ \vdots & & \vdots \\ e^{\lambda_{2n} t_1} & \dots & e^{\lambda_{2n} t_{2n}} \end{bmatrix} \\ &= \underbrace{\left[\hat{\mathbf{z}}_{(1)} \ ... \ \hat{\mathbf{z}}_{(2n)}\right]}_{\hat{\mathbf{Z}}} \underbrace{\begin{bmatrix} e^{\lambda_1 t_1} & \dots & e^{\lambda_1 t_{2n}} \\ \vdots & & \vdots \\ e^{\lambda_{2n} t_1} & \dots & e^{\lambda_{2n} t_{2n}} \end{bmatrix}}_{\mathbf{\Lambda}} \end{aligned} \tag{24}$$

Following the same reasoning for a third set of responses delayed by an interval $2\,\Delta t$ with respect to those of equation (23) yields:

$$\underbrace{[\mathbf{q}(t_1 + 2\Delta t) \ ... \ \mathbf{q}(t_{2n} + 2\Delta t)]}_{\mathbf{Q}_{2\Delta t}} = \underbrace{\left[\hat{\hat{\mathbf{z}}}_{(1)} \ ... \ \hat{\hat{\mathbf{z}}}_{(2n)}\right]}_{\hat{\hat{\mathbf{Z}}}} \underbrace{\begin{bmatrix} e^{\lambda_1 t_1} & \dots & e^{\lambda_1 t_{2n}} \\ \vdots & & \vdots \\ e^{\lambda_{2n} t_1} & \dots & e^{\lambda_{2n} t_{2n}} \end{bmatrix}}_{\mathbf{\Lambda}} \tag{25}$$

where $\hat{\hat{\mathbf{z}}}_{(i)} = \mathbf{z}_{(i)} e^{2\lambda_i \Delta t}$

By grouping equations (23) and (24), the following relationship is obtained:

$$\begin{bmatrix} \mathbf{Q} \\ \mathbf{Q}_{\Delta t} \end{bmatrix} = \begin{bmatrix} \mathbf{Z} \\ \hat{\mathbf{Z}} \end{bmatrix} \mathbf{\Lambda} \quad \text{or} \quad \mathbf{\Phi} = \mathbf{A}\mathbf{\Lambda} \tag{26}$$

Likewise, by grouping equations (24) and (25), one obtains:

$$\begin{bmatrix} \mathbf{Q}_{\Delta t} \\ \mathbf{Q}_{2\Delta t} \end{bmatrix} = \begin{bmatrix} \hat{\mathbf{Z}} \\ \hat{\hat{\mathbf{Z}}} \end{bmatrix} \mathbf{\Lambda} \quad \text{or} \quad \hat{\mathbf{\Phi}} = \hat{\mathbf{A}}\mathbf{\Lambda} \tag{27}$$

Eliminating matrix $\mathbf{\Lambda}$ between equations (26) and (27) gives:

$$\hat{\mathbf{\Phi}}\mathbf{\Phi}^{-1}\mathbf{A} = \hat{\mathbf{A}} \tag{28}$$

If $\mathbf{A} = [\mathbf{a}_1 \ ... \ \mathbf{a}_n]$ and $\hat{\mathbf{A}} = [\hat{\mathbf{a}}_1 \ ... \ \hat{\mathbf{a}}_n]$, the following equation relates each column $\mathbf{a}_i$ of $\mathbf{A}$ to the corresponding column $\hat{\mathbf{a}}_i$ of $\hat{\mathbf{A}}$

$$\hat{\mathbf{\Phi}}\mathbf{\Phi}^{-1}\mathbf{a}_i = \hat{\mathbf{a}}_i \tag{29}$$

Since $\hat{\mathbf{a}}_i = e^{\lambda_i \Delta t}\mathbf{a}_i$,

$$\hat{\mathbf{\Phi}}\mathbf{\Phi}^{-1}\mathbf{a}_i = e^{\lambda_i \Delta t}\mathbf{a}_i \tag{30}$$

This relation is an eigenvalue equation. The eigenvectors $\mathbf{a}_i$ have their first n co-ordinates equal to the eigenmodes of the structure [see equation (26)]. The eigenvalues are equal to $e^{\lambda_i \Delta t}$ where λ_i are the complex eigenvalues of the structure. Equation (28) illustrates that the order of matrix $\hat{\mathbf{\Phi}}\mathbf{\Phi}^{-1}$ should be equal to twice the number of modes excited in the measured response. To alleviate this drawback, the least-squares error minimisation method can be exploited. It allows to consider more data than the number of modes excited. $\mathbf{\Phi}$ and $\hat{\mathbf{\Phi}}$ are thus rectangular matrices and equation (30) is transformed into

$$\left[\hat{\mathbf{\Phi}}\mathbf{\Phi}^T\right]\left[\mathbf{\Phi}\mathbf{\Phi}^T\right]^{-1}\mathbf{a}_i = e^{\lambda_i \Delta t}\mathbf{a}_i \tag{31}$$

3.2 Theory of Modal Confidence Factor

The concept of assumed stations was introduced in order to avoid the use of numerous sensors. Assumed stations are generated by considering the response of the real stations $q(t)$ but delayed by an interval $\Delta\tau$

$$\begin{aligned} \mathbf{q}(t+\Delta\tau) = \mathbf{q}'(t) &= \sum_{k=1}^{2n} \mathbf{z}_{(k)}\, e^{\lambda_k (t+\Delta\tau)} \\ &= \sum_{k=1}^{2n} \mathbf{z}_{(k)}\, e^{\lambda_k \Delta\tau}\, e^{\lambda_k t} \\ &= \sum_{k=1}^{2n} \mathbf{z}'_{(k)}\, e^{\lambda_k t} \end{aligned} \tag{32}$$

and,

$$\begin{bmatrix} \mathbf{q}(t) \\ \mathbf{q}'(t) \end{bmatrix} = \sum_{k=1}^{2n} \begin{bmatrix} \mathbf{z}_{(k)} \\ \mathbf{z}'_{(k)} \end{bmatrix} e^{\lambda_k t} \tag{33}$$

Equation (33) is the response vector of a transformed system with p real stations and p assumed stations. This system has now $2p$ stations and the order of original response vector has doubled. This procedure can be extended to triple, quadruple, etc., the apparent number of stations.

Since the order of matrix $\hat{\mathbf{\Phi}}\mathbf{\Phi}^{-1}$ or $\left[\hat{\mathbf{\Phi}}\mathbf{\Phi}^T\right]\left[\mathbf{\Phi}\mathbf{\Phi}^T\right]^{-1}$ may exceed the number of modes excited in the measured response, it remains to separate the structural modes from the numerical modes related to the noise. For this purpose, the modal confidence factor (MCF) is calculated to decide whether a mode is a structural mode or not. If $\mathbf{z}_{i(k)}$ is the ith deflection of the kth mode at the real station then, from the foregoing developments, the i^{th} deflection of the kth mode at the assumed station delayed by $\Delta\tau$ is expected to be

$$\mathbf{z}_{i(k),expected} = \mathbf{z}_{i(k)}\, e^{\lambda_r \Delta\tau} \tag{34}$$

If the identified mode is a structural mode, $\mathbf{z}_{i(k),expected}$ should be equal to $\mathbf{z}'_{i(k)}$. The MCF is then defined as

$$\begin{aligned} MCF &= \left| \frac{\mathbf{z}_{i(k),expected}}{\mathbf{z}'_{i(k)}} \right| \quad \mathbf{z}'_{i(k)} > \mathbf{z}_{i(k),expected} \\ &= \left| \frac{\mathbf{z}'_{i(k)}}{\mathbf{z}_{i(k),expected}} \right| \quad \mathbf{z}_{i(k),expected} > \mathbf{z}'_{i(k)} \end{aligned} \tag{35}$$

and should be near unity.

3.3 Application to an Experimental Structure

The ITD method is applied to the analysis of the dynamic characteristics of the aeroplane-like structure (see Figure 3). Five assumed stations delayed by $\Delta\tau = 10\,\Delta t$ are considered.

Table 2 presents the natural frequencies and damping ratios. The corresponding MCFs are also listed and show that some modes are more difficult to identify than the others. The identified mode shapes are depicted in Figure 7.

Natural frequencies (Hz)	Damping ratios (%)	MCFs
4.39	$\simeq 3$	0.9-1
18.12	0.42	1
41.64	0.58	0.9-1
83.09	0.92	0.99
84.76	0.80	0.8-1
92.07	$\simeq 1.4$	0.8-1
101.52	$\simeq 0.4$	0.8-1

Table 2: Natural frequencies and damping ratios (ITD method).

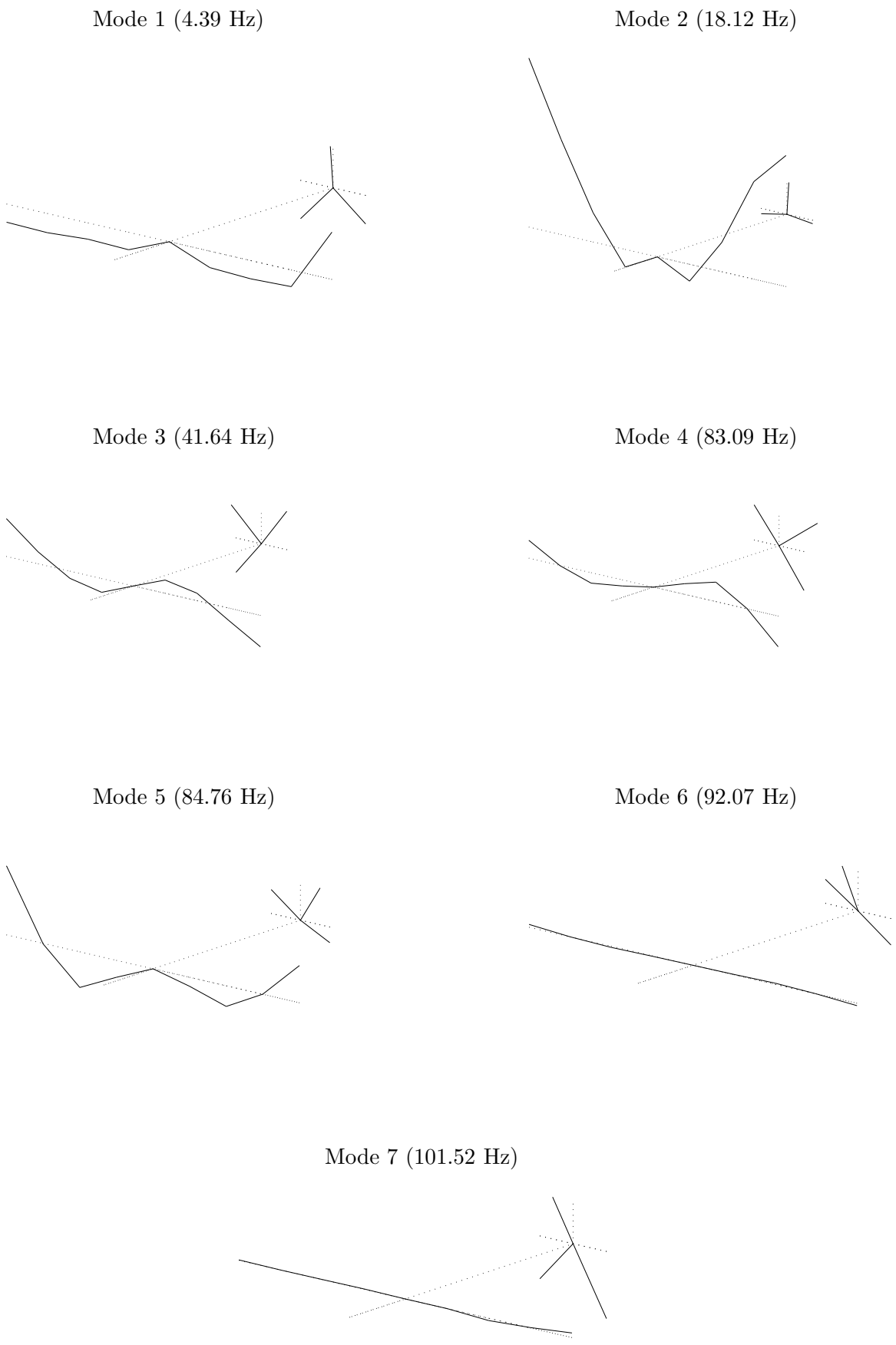

Figure 7: Representation of the mode shapes in the 0-100 Hz range (ITD method).

4 Stochastic Subspace Identification Method

4.1 Stochastic State Space Models

The Stochastic Subspace Identification method (SSI) works directly with recorded time signals. The key advantage of the method is the fact that the external forces need not to be measured as long as they are uncorrelated random signals. It should be noted that the technique can also be used to analyse data obtained from the free response of a system.

Given an n-dimensional time series $\mathbf{q}[k] = \mathbf{q}(t_k)$, the dynamic behaviour of a structure can be described by a stochastic state space formulation of the form:

$$\begin{aligned} \mathbf{r}[k+1] &= \mathbf{A}\mathbf{r}[k] + \mathbf{w}[k] && (36) \\ \mathbf{q}[k] &= \mathbf{B}\mathbf{r}[k] + \mathbf{v}[k] && (37) \end{aligned}$$

Equation (36) is called the state equation and models the dynamic behaviour of the physical system whereas equation (37) is called the observation or output equation and details which components of vector $\mathbf{r}$ are measured. The following notations are used:

- Matrices $\mathbf{A}$ and $\mathbf{B}$ are the state space and output matrices respectively;
- $\mathbf{r}[k]$ represents the state vector;
- $\mathbf{w}[k]$ and $\mathbf{v}[k]$ represent the process and measurement noises respectively.

It should be noted that the process noise drives the system dynamics whereas the measurement noise due to sensor inaccuracies is the direct disturbance of the system response. They are both assumed to be zero-mean white Gaussian noise processes with the following covariance matrices:

$$E\left[\begin{pmatrix} \mathbf{w}[k] \\ \mathbf{v}[k] \end{pmatrix} \begin{pmatrix} \mathbf{w}[k+t]^T & \mathbf{v}[k+t]^T \end{pmatrix}\right] = \begin{pmatrix} \mathbf{Q} & \mathbf{S} \\ \mathbf{S} & \mathbf{R} \end{pmatrix} \delta(t) \tag{38}$$

where E is the expectation and $\delta(t)$ is the Kronecker delta.

The output covariances matrices $\mathbf{\Lambda}_0$ and $\mathbf{\Lambda}_i$ are defined as:

$$\begin{aligned} \mathbf{\Lambda}_0 &= E[\mathbf{q}[k]\ \mathbf{q}[k]^T] \\ \mathbf{\Lambda}_i &= E[\mathbf{q}[k+i]\ \mathbf{q}[k]^T] && (39) \end{aligned}$$

As $\mathbf{w}[k]$ and $\mathbf{v}[k]$ are independent of the state vector $\mathbf{r}[k]$, the following properties can be established from equations (36) to (39):

$$\begin{aligned} E[\mathbf{r}[k]\ \mathbf{r}[k]^T] &= \mathbf{A}\mathbf{\Sigma}_0\mathbf{A}^T + \mathbf{Q} \\ E[\mathbf{r}[k+1]\ \mathbf{r}[k]^T] &= \mathbf{G} = \mathbf{A}\mathbf{\Sigma}_0\mathbf{B}^T + \mathbf{S} \\ \mathbf{\Lambda}_0 &= \mathbf{B}\mathbf{\Sigma}_0\mathbf{B}^T + \mathbf{R} \\ \mathbf{\Lambda}_i &= \mathbf{B}\mathbf{A}^{i-1}\mathbf{G} && (40) \end{aligned}$$

where $\mathbf{\Sigma}_0$ is the state covariance matrix and $\mathbf{G}$ is referred to as the next state-output covariance matrix.

4.2 Covariance-Driven Stochastic Subspace Method

Several variants of the SSI method have been proposed in the literature. In what follows, we focus on the so-called covariance-driven stochastic subspace method which is known to be simple to implement and not too much computationally demanding.

Let $\mathbf{H}_{p,q}$ be the following block-Hankel matrix filled up with p blocks rows and q block columns ($q \geq p$) of the output covariance matrix $\mathbf{\Lambda}_i$:

$$\mathbf{H}_{p,q} = \begin{bmatrix} \mathbf{\Lambda}_1 & \mathbf{\Lambda}_2 & ... & ... & \mathbf{\Lambda}_q \\ \mathbf{\Lambda}_2 & \mathbf{\Lambda}_3 & ... & ... & \mathbf{\Lambda}_{q+1} \\ ... & ... & ... & ... & ... \\ \mathbf{\Lambda}_p & \mathbf{\Lambda}_{p+1} & ... & ... & \mathbf{\Lambda}_{p+q+1} \end{bmatrix} \tag{41}$$

Let

$$\begin{aligned} \mathbf{O}_p &= \begin{bmatrix} \mathbf{B} & \mathbf{BA} & ... & \mathbf{BA}^{p-1} \end{bmatrix}^T \\ \mathbf{C}_q &= \begin{bmatrix} \mathbf{G} & \mathbf{AG} & ... & \mathbf{A}^{q-1}\mathbf{G} \end{bmatrix} \end{aligned} \tag{42}$$

be the pth-order observability and controllobility matrices respectively. They are assumed to be of rank $2N_m$, where N_m is the number of system modes. The last relationship of equation (40) leads to the following well known factorisation property:

$$\mathbf{H}_{p,q} = \mathbf{O}_p \, \mathbf{C}_q \tag{43}$$

Let $\mathbf{W}_1$ and $\mathbf{W}_2$ be two user-defined invertible weighting matrices of size $p\,m$ and $q\,m$ respectively where m is the dimension of the response vector $\mathbf{q}[k]$. Performing the singular value decomposition of the weighted Hankel matrix gives:

$$\mathbf{W}_1\mathbf{H}_{p,q}\mathbf{W}_2 = \begin{bmatrix} \mathbf{U}_1 & \mathbf{U}_2 \end{bmatrix} \begin{bmatrix} \mathbf{S}_1 & \mathbf{0} \\ \mathbf{0} & \mathbf{0} \end{bmatrix} \begin{bmatrix} \mathbf{V}_1 & \mathbf{V}_2 \end{bmatrix}^T = \mathbf{U}_1 \, \mathbf{S}_1 \, \mathbf{V}_1^T \tag{44}$$

where $\mathbf{S}_1$ contains $n = 2N_m$ non-zero singular values in decreasing order. The system order can then be determined as the number of non-zero singular values of the weighted Hankel matrix. Different choices of the weighting matrices lead to different identification methods. Here we consider an unweighted approach:

$$\mathbf{W}_1 = \mathbf{W}_2 = \mathbf{I} \tag{45}$$

From equations (43) and (44), the observability and controllability matrices can be recovered, up to a similarity transformation:

$$\begin{aligned} \mathbf{O}_p &= \mathbf{U}_1 \, \mathbf{S}_1^{1/2} \\ \mathbf{C}_q &= \mathbf{S}_1^{1/2} \, \mathbf{V}_1^T \end{aligned} \tag{46}$$

If $\mathbf{O}_p^{\uparrow}$ is the upper-shifted $\mathbf{O}_{p-1}$ matrix by one block row, one obtains:

$$\mathbf{O}_p^{\uparrow} = \begin{bmatrix} \mathbf{BA} & \mathbf{BA}^2 & ... & \mathbf{BA}^{p-1} \end{bmatrix}^T = \mathbf{O}_{p-1}\mathbf{A} \tag{47}$$

Matrices $\mathbf{O}_p^{\uparrow}$ and $\mathbf{O}_{p-1}$ being determined by making use of $\mathbf{O}_p$ matrix, the state matrix $\mathbf{A}$ can be easily computed as the solution of equation (47). Matrix $\mathbf{B}$ is merely equal to the first block row of $\mathbf{O}_p$.

The mode shape Ψ_r of the r^{th} mode at the sensor locations are the observed parts of the system eigenvectors Φ_r of A, given by the following equation :

$$\psi_r = [B]\Phi_r \tag{48}$$

These relations correspond to the complex mode shapes of the structure and the corresponding eigenvalues λ_i are related to the system poles μ_i by the relationship:

$$\lambda_i = e^{\mu_i \, \Delta t} \tag{49}$$

4.3 In Practice

It is emphasised that all the previous developments hold for 'true' block Hankel matrices and for a finite system order. In practice, a mechanical system has an infinite order and the 'true' covariance functions defined in equation (39) are unknown. However, an unbiased estimate of the covariance matrix is given by:

$$\hat{\mathbf{\Lambda}}_i = \frac{1}{N-i} \sum_{k=0}^{N-i-1} \left(\mathbf{q}[k+i]\mathbf{q}[k]^T \right) \quad \text{pour} \quad 0 \leq i < N-1 \tag{50}$$

where N is the number of observations.

The singular value decomposition of the estimated Hankel matrix will then give:

$$\hat{\mathbf{H}}_{p,q} = \begin{bmatrix} \hat{\mathbf{U}}_1 & \hat{\mathbf{U}}_2 \end{bmatrix} \begin{bmatrix} \hat{\mathbf{S}}_1 & \mathbf{0} \\ \mathbf{0} & \hat{\mathbf{S}}_2 \end{bmatrix} \begin{bmatrix} \hat{\mathbf{V}}_1 & \hat{\mathbf{V}}_2 \end{bmatrix}^T \tag{51}$$

with:

$$\begin{aligned} \hat{\mathbf{S}}_1 &= \text{diag}(\sigma_1, ..., \sigma_n), \quad \sigma_1 \geq \sigma_2 \geq ... \geq \sigma_n \\ \hat{\mathbf{S}}_2 &= \text{diag}(\sigma_{n+1}, ..., \sigma_{pm}), \quad \sigma_{n+1} \geq \sigma_{n+2} \geq ... \geq \sigma_{pm} \end{aligned} \tag{52}$$

The model order is generally selected so that $\sigma_n >> \sigma_{n+1}$. The Hankel and observability matrices are then approximated by:

$$\begin{aligned} \hat{\mathbf{H}}_{p,q} &= \hat{\mathbf{U}}_1 \hat{\mathbf{S}}_1 \hat{\mathbf{V}}_1^T \\ \hat{\mathbf{O}}_p &= \hat{\mathbf{U}}_1 \hat{\mathbf{S}}_1^{1/2} \end{aligned} \tag{53}$$

In practice, a significant drop in the singular values cannot always be observed. In this case, the problem of order determination is solved by plotting a stabilisation diagram for increasing model orders.

4.4 Application to an Experimental Structure

As for the two previous methods, the SSI method is applied to the aeroplane-like structure. Table 3 and Figure 8 show the results obtained.

A quick look at Tables 1, 2 and 3 enables us to conclude that the natural frequencies and damping ratios estimated by the three methods are in very good agreement. A qualitative comparison of the mode shapes confirm this finding. However, a more precise comparison would be obtained using a quantitative measure of the agreement between the modes. This is discussed in the next section.

Natural frequencies (Hz)	Damping ratios (%)
4.42	$\simeq$3
18.12	0.41
41.64	0.56
83.09	0.93
84.76	0.81
92.12	$\simeq$1.4
101.60	0.45

Table 3: Natural frequencies and damping ratios (SSI method).

5 Modal Assurance Criterion

A widely used technique for comparing mode shapes is the modal assurance criterion (MAC) [12]. It gives quantitatively a good idea of the closeness between two families of mode shapes $\mathbf{x}^{\{1\}}$ and $\mathbf{x}^{\{2\}}$:

$$\mathrm{MAC}(\mathbf{x}_{(i)}^{\{1\}}, \mathbf{x}_{(j)}^{\{2\}}) = \left(\frac{\mathbf{x}_{(i)}^{\{1\}^T} \mathbf{x}_{(j)}^{\{2\}}}{\|\mathbf{x}_{(i)}^{\{1\}}\| \|\mathbf{x}_{(j)}^{\{2\}}\|} \right)^2 \tag{54}$$

In this equation, the MAC is computed between mode i of the first family and mode j of the second family. MAC values oscillate between 0 and 1, a unitary value meaning a perfect correlation. In practice, a value greater to 0.9 is commonly recognised as acceptable to establish the correspondence between two mode shapes.

Generally speaking, the MAC matrix is used for the comparison of the modes identified from the measured data (i.e. experimental model analysis) and the modes computed from the analytical model (i.e. theoretical model analysis). Here, it is exploited in order to compare the modes identified using the three identification techniques. The comparison is represented in Figure 9. Two remarks may be drawn regarding this figure:

- A very good concordance is obtained between the mode shapes identified using SSI and ITD methods;
- The concordance is a bit less good with the modes obtained using LSFD method especially for the first and seventh modes.

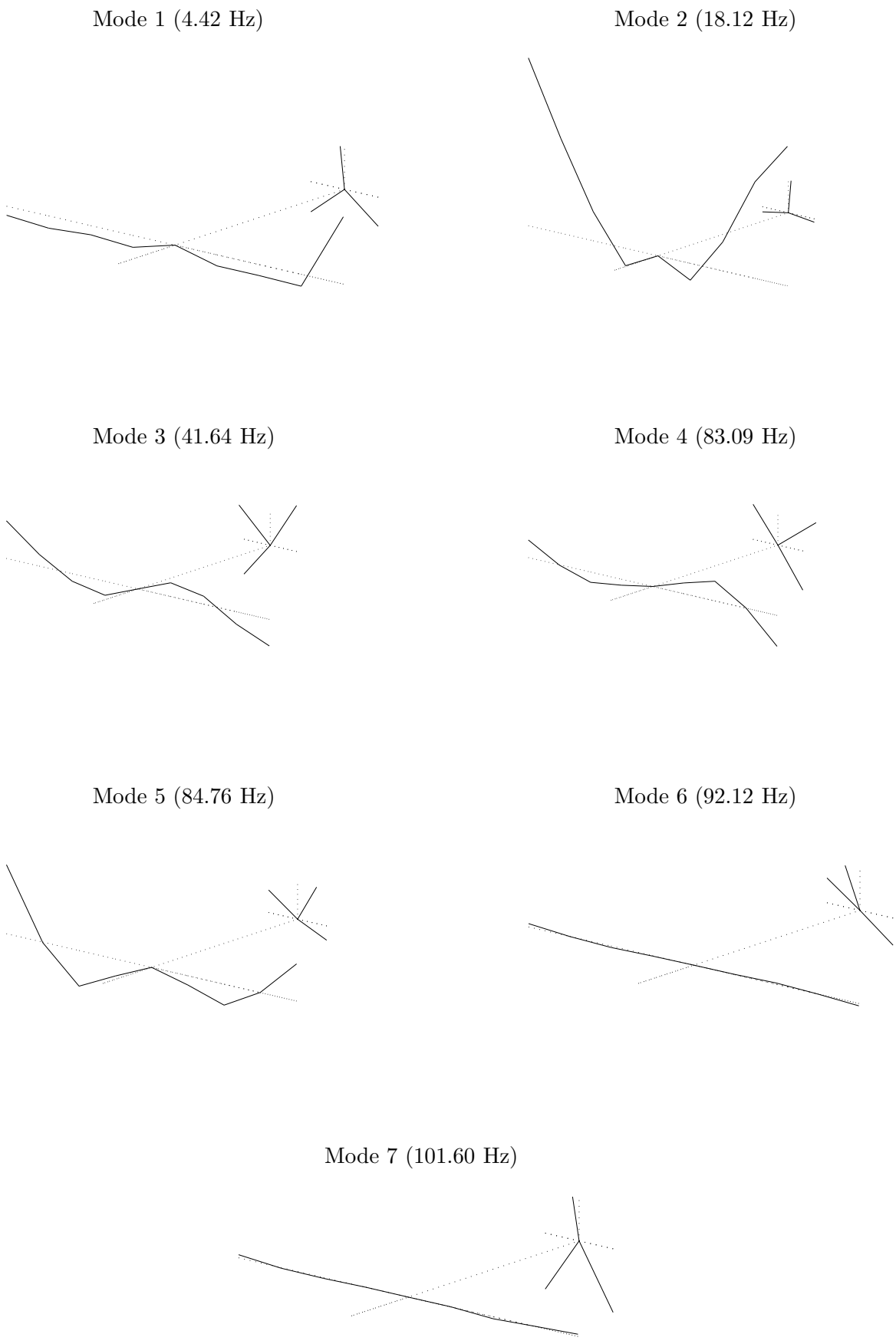

Figure 8: Representation of the mode shapes in the 0-100 Hz range (SSI method)

Attention should be paid to the number of degree-of-freedom in the mode shapes being compared. If it is relatively low, a mode of family 1 may appear to correlate equally well with several modes of family 2. This problem is a spatial version of aliasing. In this case, there are insufficient measured degree-of-freedom in order to discriminate between the different modes. The only solution is to measure more degree-of-freedom. However, the MAC can tell us whether there are enough measurement points. This is done using a version of the MAC called the AutoMAC in which a set of modes are correlated with themselves. The AutoMAC is illustrated in Figure 10 for the modes extracted from the SSI method. The off-diagonal terms are not too high indicating that enough sensors have been considered.

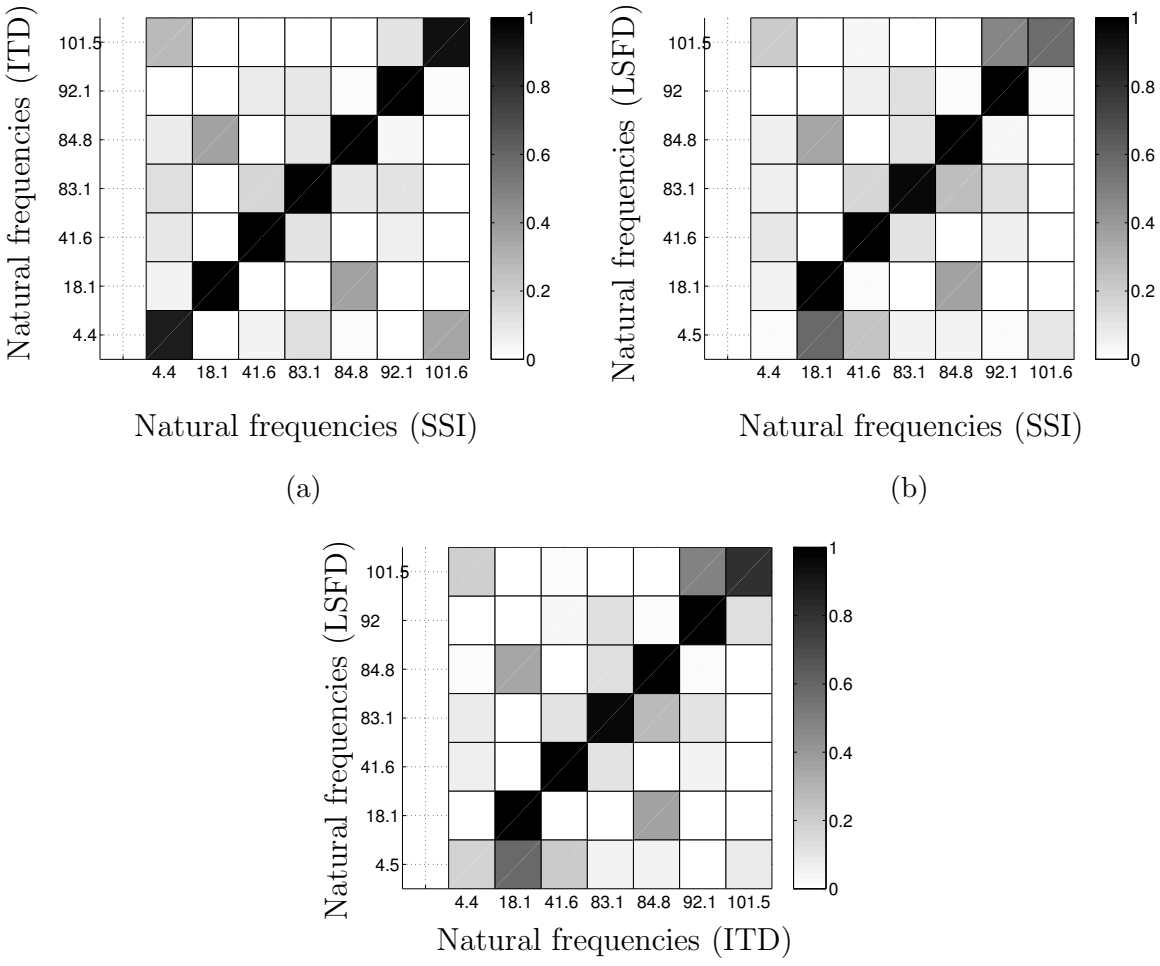

Figure 9: Comparison of the three sets of identified modes. (a) SSI vs. ITD; (b) SSI vs. LSFD; (c) ITD vs. LSFD.

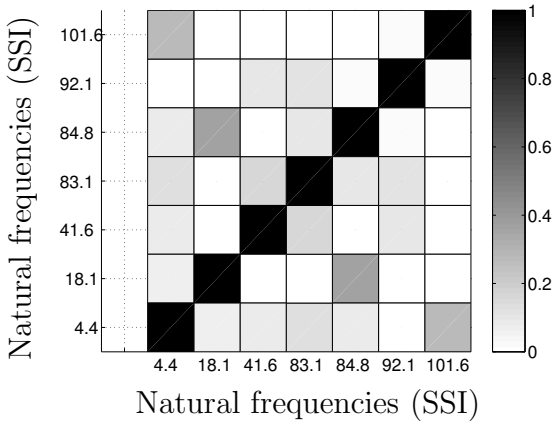

Figure 10: AutoMAC (SSI method)

References

[1] D.J. Ewins 2000 *Modal Testing: Theory, Practice and Application*. Baldock: Research Studies Press LTD, 2nd edition.

[2] W. Heylen, S. Lammens and P. Sas 1997 *Modal Analysis Theory and Testing*. Leuven: KUL Press.

[3] N.M.M. Maia and J. M.M. Silva 1997 *Theoretical and Experimental Modal Analysis* Taunton: Research Studies Press LTD.

[4] R.E Melchers 1999 *Structural Reliability Analysis and Prediction*. Chichester: John WIley & sons, 2nd edition.

[5] S.W. Doebling, C.R. Farrar and M.B. Prime 1999 *Shock and Vibration Digest* **205**, 631-645. A summary review of vibration-based damage identification techniques.

[6] M.I. Friswell and J.E. Mottershead 1995 *Finite Element Model Updating in Structural Dynamics*. London: Kluwer Academic Publishers.

[7] D.L. Brown, R.J. Allemang, R. Zimmerman and M. Mergeay 1979 *SAE Technical Paper Series* No. 790221. Parameter estimation techniques for modal analysis.

[8] S.R. Ibrahim and E.C. Mikulcik 1973 *The Shock and Vibration Bulletin* **43**, 21-37. A time domain modal vibration test technique.

[9] P. Van Overschee and B. De Moor 1996 *Subspace Identification for Linear Systems: Theory, Implementation, Applications* Dordrecht: Kluwer Academic Publishers.

[10] M. Link and M.I. Friswell 2003 *Mechanical Systems and Signal Processing* **17**, 9-20. Working group 1: Generation of validated structural dynamics models - Results of a benchmark study utilising the GARTEUR SM-AG19 test-bed.

[11] M. Geradin and D. Rixen 1994 *Mechanical Vibrations, Theory and Application to Structural Dynamics*. Paris, France: Masson.

[12] R. Allemang and D. Brown 1982 *Proceedings of the 1st International Modal Analysis Conference*, Orlando, 110-116. A correlation coefficient for modal vector analysis.